Avrupa Bilim ve Teknoloji Dergisi
Sayı 50, S. 36-46, Nisan 2023

Araştırma Makalesi

www.ejosat.com ISSN:2148-2683

European Journal of Science and Technology
No. 50, pp. 36-46, April 2023

Research Article

Choline Chloride Encapsulated PLGA Nanoparticles Labelled with Lanthanide Metals

Burcu Ucar

Department of Biomedical Engineering, Faculty of Engineering and Architecture, Istanbul Arel University, Istanbul 34537, Turkey (ORCID: 0000-0002-8540-7832), brccr87@gmail.com

(İlk Geliş Tarihi 31 Ekim 2022 ve Kabul Tarihi 20 Şubat 2023)

(**DOI:** 10.31590/ejosat.1197269)

ATIF/REFERENCE: Ucar, B. (2023). Choline Cloride Encapsulated PLGA Nanoparticles Labelled with Lanthanide Metals. European Journal of Science and Technology, (50), 36-46.

Abstract

Herein, choline chloride was loaded into PLGA nanoparticles to ensure its controlled release. Encapsulation efficiencies (EE) and loading capacities (LC) of them were determined. Also, the produced nanoparticles were analyzed with Zetasizer, FT-IR, SEM, and XRD. The surfaces of the nanoparticles were functionalized by labeling with three different natural lanthanide metals Europium, Gadolinium, and Lutetium to expand diagnostic and therapeutic capabilities with three different imaging techniques. Metal labeling of the nanoparticles was confirmed with SEM-EDX analysis. EE of the choline chloride nanoparticles were ranging between 62.5%-88.9%. LC of the choline chloride nanoparticles varied from 34.9 to 61.4. The mean size distribution obtained from the Zetasizer analysis of the free nanoparticles was 261.0 ± 7.598 nm. The Z-average size of the encapsulated nanoparticles also varied from 257.5 to 270 nm. The quite negative zeta potential, for example, -17.85 ± 0.165 mV for free NPs showed that the nanoparticles were sufficiently stable. The elemental mapping of the metal labeled NPs verified the labeling procedure. By obtaining therapeutic choline chloride-loaded nanoparticles with different metal labels, theranostic agents with common target and the ability to eliminate limitations with different imaging and detection techniques have been produced.

Keywords: Choline chloride, PLGA, Lanthanides.

Lantanit Metallerle İşaretlenmiş Kolin Klorür Enkapsüle PLGA Nanopartikülleri

Öz

Burada, kolin klorür kontrollü salımın sağlanması için PLGA nanoparçacıklarına yüklenmiştir. Bunların kapsülleme verimleri (EE) ve yükleme kapasiteleri (LC) belirlenmiştir. Ayrıca üretilen nanopartiküller Zetasizer, FT-IR, SEM ve XRD ile karakterize edilmiştir. Nanopartiküllerin yüzeyleri, üç farklı görüntüleme tekniği ile tanı ve tedavi kapasitesini genişletmek için üç farklı doğal lantanit metali Europium, Gadolinium ve Lutetium ile işaretlenerek işlevselleştirilmiştir. Nanopartiküllerin metal işaretlemesi SEM-EDX analizi ile doğrulanmıştır. Kolin klorür yüklü nanoparçacıkların EE'si %62.5-%88.9 arasında değişmiştir. Kolin klorür yüklü nanoparçacıkların LC'si %34.9 ile %61.4 arasında değişmiştir. Serbest nanopartiküllerin Zetasizer analizinden elde edilen ortalama boyut dağılımı 261.0 ± 7.598 nm idi. Kapsüllenmiş nanoparçacıkların Z-ortalama boyutu da 257.5 ila 270 nm arasındaydı. Oldukça negatif zeta potansiyeli, örneğin, serbest NP'ler için -17.85 ± 0.165 mV, nanoparçacıkların yeterince kararlı olduğunu göstermiştir. Metal işaretli NP'lerin element haritalaması, işaretleme prosedürünü doğrulamıştır. Terapötik kolin klorürür yüklü farklı metal işaretli nanoparçacıkların elde edilmesi ile aslında ortak hedefe yönelik ve farklı görüntüleme ve dedeksiyon teknikleri ile limitasyonları ortadan kaldırma beceresine sahip teranostik ajanlar üretilmiştir.

Anahtar Kelimeler: Kolin klorür, PLGA, Lantanitler.

1. Introduction

Choline chloride (ChCl) (Figure 1) is a quaternary ammonium base (Kuang et al., 2010) and significant as an requisite nutrient for sustaining normal liver function of cells (Kuang et al., 2010; Liu et al., 2020; O'Dwyer et al., 2020). According to the results of different studies; Choline shortage can bring about varying degrees of liver damage, liver cirrhosis, dyslipidemia, and liver cancer (Higdon, Drake, Delage, & Stocker, 2000; Lau, Zhang, & Yu, 2017; Liu et al., 2020; Marcolin et al., 2011; Mehedint & Zeisel, 2013). Liver malignancy and its predominant type, HCC (hepatocellular carcinoma) is one of the most common malignancies with an increasing incidence worldwide (Cicalese, 2022; NORD, 2017; Philips et al., 2021). Based on the liver cancer 2020 data reported by the World Health Organization (WHO); the global incidence is estimated at 905,677 and the death rate at 830,180 (WHO, 2020). The disease still has a poor prognosis in the range of 5-30% with five-year survival (Liu et al., 2020; Philips et al., 2021). It is also estimated that more than one million people will be affected by liver cancer each year by 2025 (Philips et al., 2021). Although hepatitis viral infections are responsible for this increase due to approximately 50% case rate (Kuang et al., 2010; Liu et al., 2020), severely insufficient dietary choline intake of the Chinese population cannot be excluded due to the case rate of approximately 45% (Llovet et al., 2022). The $^{99}Tc^{m}$-Colloid (TIN) SPECT imaging technique is routinely applied to determine the organ size and presence of focal lesions and the degree of hepatocellular dysfunction in liver diseases (Willyard & Kalathil, 2020). According to the results of a study examining the metabolic distribution of choline using this agent; Choline absorbed from the intestine is first deposited in the liver, then recycled and redistributed from the lungs, kidneys and intestines to the liver and brain in case of insufficient choline intake. This dynamic distribution plays a role in the synthesis of phosphatidylcholine (which makes up nearly half of cell membranes) and in repairing existing damage to hepatic reticuloendothelial function. Consequently, this repair prevents the shift of colloidal choline from the liver to the spleen, increasing liver uptake and reducing splenic uptake (Al-Saeedi & Cheng, 2013; Willyard & Kalathil, 2020). All cells use choline for the biosynthesis of phospholipids (for example, PtdCho) and as a component of phosphatidylcholine to maintain the functions and structural integrity of their cell membranes (Gibellini & Smith, 2010; Liu et al., 2020). In addition, rapidly proliferating tumors are known to contain abundant phospholipids and phosphatidylcholine (PtdCho) (Glunde, Bhujwalla, & Ronen, 2011; Kuang et al., 2010). In hepatocytes and kidney cells, choline is converted to betaine by the choline oxidase enzyme system and can be oxidized to betaine aldehyde, which is the main source of the betaine methyl group (Kuang et al., 2010; Liu et al., 2020). In a study on choline supplementation, it was determined that the mentioned oxidation pathway increases DNA methylation and DNA methyltransferase expression, and plays a critical role in DNA and histone methylation homeostasis (Liu et al., 2020). It has also been noted that choline may be a critical supplement in both hepatocarcinogenesis and liver cancer survival, and may even cause a higher survival rate in HCC cases accompanied by higher serum choline levels in the case of systemic inflammation (CRP level > 3.0 mg/L) (Liu et al., 2020). According to the Positron Emission Tomography (PET) study, in which up-regulated choline uptake was used as a diagnostic marker and HCC cells was targeted, it has been reported that carcinogenesis is associated with up-regulated choline kinase activity, and this activity causes an increase in phosphocholine levels (Kuang et al., 2010). In a study based on ^{1}H and ^{31}P magnetic resonance spectroscopy (MRS), it was emphasized that choline transport and phosphorylation are faster during hepatocarcinogenesis, and that increased phosphocholine cycles may cause increased MRS values in cancer cells (Kuang et al., 2010).

These complex biodistribution studies have been simplified by the using of polymeric nanoparticles that allow different therapeutic agents reach their targets more effectively (Snehalatha, Venugopal, Saha, Babbar, & Sharma, 2008). As mentioned, the charged nanoparticles mainly accumulate in the liver and spleen, where they are transported to the bloodstream, where they are then opsonized by the macrophages of the mononuclear phagocyte system (MPS) and thus largely cleared. In this way, other organs are protected from acute toxicity (Snehalatha et al., 2008). This distribution route can be chosen in the chemotherapeutic treatment of tumors such as hepatocarcinoma or hepatic metastases (Snehalatha et al., 2008). Reddy et al. (2004) reported the biodistribution of radiolabeled etoposide-loaded lipid nanoparticles with this technique (Snehalatha et al., 2008). The development of metal-based biomaterials (especially by labeling with Lanthanides) targeting cancerous cells provides models for many pharmaceuticals, from imaging agents (radionuclides, magnetic, fluorescent) to contrast and chemotherapeutic agents (Dasari & Patra, 2015; Tikhonova, Shirshin, Budylin, Fadeev, & Petrova, 2014; B. Ucar & Acar, 2021). Developed as luminescent bioprobes, magnetic resonance imaging (MRI) agents, biologically responsive cellular imaging agents, and targeted radionuclide therapy agents, these agents are gaining increasing popularity as simulating agents prior to clinical application (B. Ucar & Acar, 2021). The radioisotope ^{177}Lu of lutetium(III) chloride is used in the theranostic-based treatment of cancer types including prostate, multiple myeloma, neuroendocrine tumors and metastases, but radiolabeling is clinically possible in Nuclear Medicine Departments (Demirkol et al., 2018; Demirkol, Özkan, Uçar, Wester, & Ferhanoğlu, 2021; Kierkowicz et al., 2017; Özkan et al., 2020).

The technique to be applied using each imaging agent produced in this study has advantages and limitations, so they are considered to be complementary to each other (Greiser, Weigand, & Freesmeyer, 2019). Metal-based colloids used in MRI and SPECT represent an important branch of clinically relevant liver-specific pharmaceuticals (Greiser et al., 2019), while fluorescent-based colloids guide more sensitive tumor resection operations (Han, Deng, Sun, Ling, & Shen, 2015). MRI provides sub-millimetre resolution images of soft tissue structures with high-contrast anatomical information, while scintigraphy or SPECT primarily provides functional images (Greiser et al., 2019). Radiolabeled colloid scintigraphy is still used to determine regional liver function with SPECT and to identify common liver diseases such as cirrhosis (Greiser et al., 2019). The trivalent gadolinium ion (Gd^{3+}), routinely used in MR imaging, has seven unpaired electrons in its outer electron shell and is highly paramagnetic (Cebeci, Ucar, Acar, & Erden, 2021; Han et al., 2015). Eu^{3+} has high paramagnetism with six unpaired electrons in its outer electron shell (Han et al., 2015). However, its use in MRI is limited due to its poor stabilization. Eu^{3+} has long radiative emission lifetimes with f→f transitions, is photoluminescent, emits long-lived effective fluorescence (585-630 nm, red), and has low toxicity (Han et al., 2015). ^{177}Lu is an important therapeutic radioisotope with widespread use in Targeted Radionuclide Therapy (TRT) (Dash, Pillai, & Knapp, 2015;

Demirkol et al., 2018; Kierkowicz et al., 2017). The mean penetration range of β^- particles emitted by ^{177}Lu in soft tissue is 670 μm, making this radionuclide perfect for transmitting energy to small volumes such as micrometastatic disease (less than 3 mm in diameter) (Dash et al., 2015). Moreover, localizing cytotoxic radiation at micro dimensions, ^{177}Lu thus, destroys small tumors and metastatic lesions while preserving normal tissue (Dash et al., 2015). Low-energy gamma photons of ^{177}Lutetium allow imagination of its biodistribution and pharmacokinetics with the same radiolabelled pharmaceutical used for therapy (theranostics for personalized medicine) (Dash et al., 2015; Demirkol et al., 2021; Özkan et al., 2020). Lutetium exists only in the +3 oxidation state, does not undergo reduction-oxidation complications, and generally forms nine coordination complexes (Dash et al., 2015). ^{177}Lu has a long time period with a half-life of 6.65 days (Dash et al., 2015). Lutetium(III) chloride, its radioisotope ^{177}Lutesium, is used in the theranostic-based treatment of cancer types including prostate, multiple myeloma, neuroendocrine tumors and metastases, but radiolabeling is clinically possible in the Nuclear Imaging Departments. The imaging agents produced in this study target the RES and therefore show minimal biliary excretion. They accumulate in Kupffer cells, thus visualizing heterogeneities in liver uptake and aggregation defects (Greiser et al., 2019).

In this study, basically, choline, which is known to have both therapeutic and protective effects against hepatic reticuloendothelial function damage such as HCC, liver leakage, and cirrhosis, was loaded on PLGA nanoparticles, and labeled with Gadolinium, Lutetium and Europium to examine the therapeutic effect, biodistribution and pharmacokinetic properties of these loaded nanoparticles. Thus, technique-specific limitations can be avoided by evaluating different imaging modalities such as MRI, SPECT, and fluorescence imaging separately.

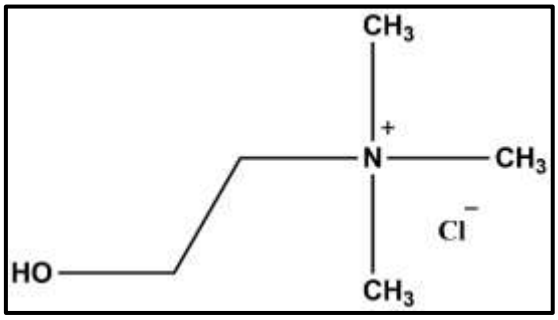

Figure 1. Molecular structure of the choline chloride

PLGA (Figure 2) is a FDA (Food and Drug Administration)-approved, biocompatible and biodegradable polymer. It is a system that is frequently preferred in providing controlled release of many different active ingredients, increasing its bioavailability and cellular response, and improving its cytotoxic activity. The most widely used method for loading hydrophilic active ingredients into PLGA nanoparticles is the double emulsion solvent evaporation method. PLGA can be easily hydrolyzed in water and its hydrolysis products can be broken down to CO_2 and H_2O by metabolic pathway (Figure 2) (Makadia & Siegel, 2011; Tosyali et al., 2021).

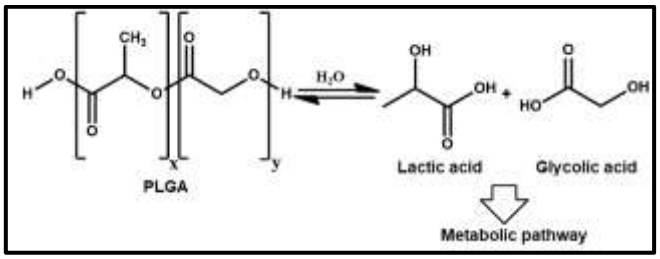

Figure 2. Molecular structure of the PLGA and its hydrolysis

2. Material and Method

2.1. Material

Choline chloride (ChCl) was gifted from Dr. Melih Besir Arvas, Ph.D.. PLGA, $EuCl_3.6H_2O$, $GdCl_3.6H_2O$, $LuCl_3$ and other solvents were obtained from Sigma Aldrich. Ultra pure water produced from Elix-70 system.

2.2. Method

2.2.1. Production of the Nanoparticles

Choline chloride is a very water-soluble molecule (Arias et al., 2020). Encapsulation of ChCl into polymeric nanoparticles was performed by double emulsion (water/oil/water, w/o/w) solvent evaporation method based on previous works with minor modifications (Abamor et al., 2019; Tosyali et al., 2021).

25-100 mg of the ChCl was dissolved in 850 μL dH_2O. This solution was added dropwise to the solution of 100 mg of PLGA dissolved in 1.5 mL of DCM and 90 seconds 80% of amplitude sonication was applied using a probe sonicator (Bandelin). Thus, the first emulsion w/o was prepared. For the second emulsion, the obtained w/o phase was added dropwise with a syringe to freshly prepared 8 mL of 3% PVA. PVA is one of the most frequently utilized polymeric surfactants to stabilize the obtained emulsion. Lastly,

the formed $w_1/o/w_2$ emulsion was added dropwise to 35 mL of 0.1% (w/v) PVA solution. It was stirred at 400 rpm at room temperature for two hours to allow the DCM to evaporate. The formed NPs were washed three times with distilled water followed by centrifugation at 9000 rpm for 30 min at 4 °C to remove the PVA and the non-encapsulated ChCl from the outer aqueous phase. Lastly, the NPs were lyophilized and stored at -18 °C until use.

2.2.2. Characterization of the Nanoparticles

DLS and ELS measurements of the NPs were performed with Zetasizer (Malvern, Nano ZS). FT-IR spectra were obtained from Shimadzu IR-prestige in the range of 650-4000 cm^{-1}. The morphology and elemental structure of the NPs were investigated utilizing scanning electron microscopy (SEM, Zeiss EVO® LS 10 SEM) and energy dispersive spectra (EDS, Zeiss EVO® LS 10 SEM), respectively. Powder X-ray diffraction analyses of the produced NPs were conducted with an X-ray diffractometer (PANalytical) using Cu Kα (λ = 0.154 nm) radiation. The diffractograms were recorded in 2θ range between 5° and 90° (Acar & Ucar, 2022; Yazar, Arvas, & Sahin, 2022).

Encapsulation efficiency (EE) and loading content (LC) of ChCl were determined by the indirect method. The supernatant obtained from the washing process was centrifuged in a membrane centrifuge tube (Millipore 5kDa) at 6000 rpm for 45 minutes and analyzed in the LC-ESI-MS. The EE and LC of ChCl were calculated using the equation 1 and 2, respectively (Acar & Ucar, 2022). The calibration curve obtained for this calculation was expressed in Figure 3 [intercept: 1.43E6 ± 7005.11, slope: 953162.18 ± 33915.62].

$$EE\% = \frac{amount\ of\ the\ ChCl\ in\ the\ NPs}{amount\ of\ the\ initially\ used\ ChCl} x100 \quad [1]$$

$$LC\% = \frac{amount\ of\ the\ ChCl\ in\ the\ NPs}{amount\ of\ the\ lyophilized\ NPs} x100 \quad [2]$$

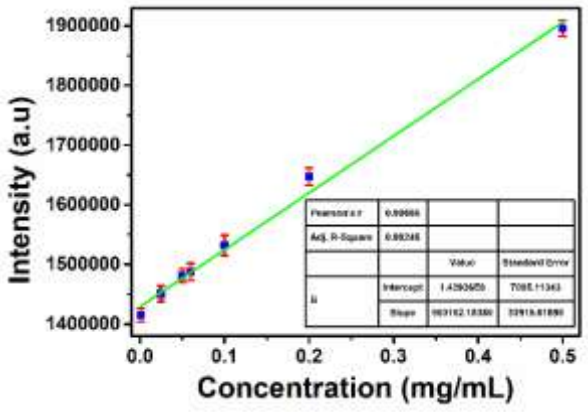

Figure 3. LC-ESI-MS calibration curve of the ChCl

The in-vitro release profiles of the ChCl loaded NPs were examined at pH 7.2 in phosphate-buffered saline (PBS). 10 mg of the NPs were redispersed in 5 mL of PBS using a bath-type sonicator (Bandelin) and incubated at 37 °C in a shaking water bath. At certain time intervals (1., 6., 24. h; 7., 14., 30. days), the samples were centrifuged at 9000 rpm for 15 minutes, and supernatants were separated. 75 µL of them were injected into an LC-MS apparatus and the amount of the released ChCl was calculated using calibration curve of the ChCl (R^2: 0.996) prepared with the LC-MS analyses (Acar & Ucar).

2.2.3. Labelling of the Nanoparticles

The nanoparticles produced using four different amounts of ChCl were labeled with three different metals. For this purpose, $5x10^{-5}$ M $EuCl_3.6H_2O$, $GdCl_3.6H_2O$, and $LuCl_3$ were prepared. 10 mg of lyophilized ChCl loaded nanoparticles (C1-C4) were redispersed with 9 mL of ammonium acetate buffer (pH 4-5). 1 mL of metal solution in ammonium acetate buffer was added and incubated for 1 hour. Metal labeled ChCl loaded nanoparticles were collected with centrifugation at 9000 rpm for 5 minutes. The obtained nanoparticles were washed with distilled water under the above-mentioned centrifugation conditions. The purified nanoparticles were redispersed with some distilled water and lyophilized (Burcu Ucar, 2019; B. Ucar & Acar, 2021).

3. Results and Discussion

3.1. Production and Characterization of the Nanoparticles

Information about the obtained nanoparticles were given in Table 1. The RY for the production of C1-C4 nanoparticles varied from 27% to 48%. As the amount of the ChCl increased, the % RY yield increased as expected.

While the amount of ChCl used initially in the C1-C3 formulations increased, EE increased. In the C4 formulation using 100 mg ChCl, the encapsulation level reached maximum. For this reason, there was no further increase in % EE. The loading capacity also

increased with the increase in the amount of ChCl. These results in EE and LC were consistent with literature studies (Acar & Ucar, 2022; Dangi & Shakya, 2013; Makadia & Siegel, 2011; Tosyali et al., 2021).

The size, PDI, and zeta potential values of the produced nanoparticles were presented in Table 2. While there was no substantial change in the size values with the increase of the amount of ChCl used at the beginning, the size of the ChCl encapsulated nanoparticles increased slightly compared to the free one. Due to the high water solubility of the molecule (~500 mg/mL) used in the study, the amount of the substance between 25-100 mg used in the formulations did not cause excessive growth in the size of the nanoparticles. The PDI value of all nanoparticles was found below 0.2, which indicates a narrow range close to monodisperse. There was no meaningful difference between the zeta potential values of the free and ChCl loaded NPs. This showed that there was no surface adhesion.

Table 1. The reaction yield (RY), encapsulation efficiency (EE), and loading content (LC) information of the nanoparticle formulations produced in the study

Formulation	**Amount of the ChCl (mg)**	**RY (%)**	**EE (%)**	**LC (%)**
C1	25	27.5	62.5	34.9
C2	50	33.1	75.8	50.4
C3	75	38.0	87.7	52.6
C4	100	44.8	88.9	61.4
Free NPs	-	52.0	-	-

Table 2. The size, PDI, and zeta potential values of the produced nanoparticles

Formulation	**Size (nm)**	**PDI**	**Zeta Potantial (mV)**
C1	270.0 ± 1.997	0.198 ± 0.015	-18.50 ± 0.863
C2	266.0 ± 2.205	0.182 ± 0.027	-15.42 ± 0.221
C3	257.5 ± 4.020	0.190 ± 0.008	-16.09 ± 0.068
C4	262.3 ± 0.987	0.194 ± 0.023	-19.83 ± 0.135
Free NPs	261.0 ± 7.598	0.199 ± 0.036	-17.85 ± 0.165

Zetasizer measurement result graphics of the NPs were presented in Figure 4 so as to support the size values given in Table 2 and present the Z-average size distributions of the NPs.

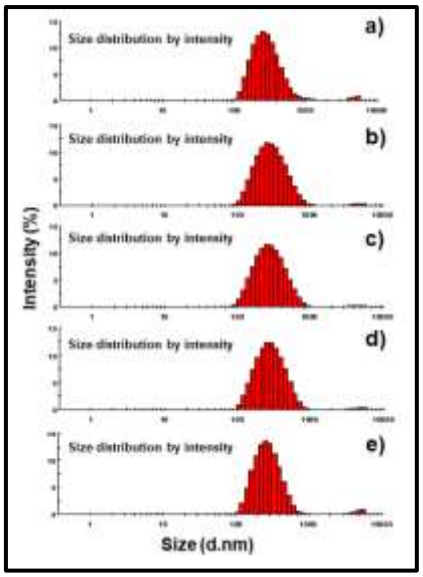

Figure 4. Particle size distributions by the intensity of the a) C1 NPs, b) C2 NPs, c) C3 NPs, d) C4 NPs, and e) free NPs

As seen in Figure 5, the O-H stretching band at 3325.28 cm^{-1}, the methyl C-H bending at 1479.40 cm^{-1}, and the C-N stretching band at 1082.06 cm^{-1} support the ChCl structure (Sivrikaya, 2019; Ullah et al., 2015). In addition to the absence of the above-mentioned bands in the spectrums of ChCl loaded nanoparticles, the same characteristics of the spectra of free and ChCl loaded nanoparticles (C1-C4) have proven that there was no surface adhesion and that encapsulation of the ChCl has taken place successfully.

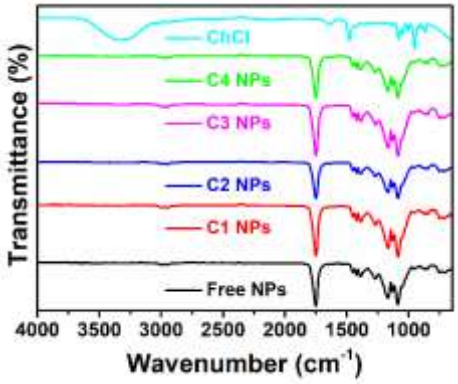

Figure 5. FT-IR spectra of the ChCl, ChCl loaded NPs (C1-C4), and free NPs

XRD patterns of the empty and ChCl loaded NPs were given in Figure 6. The literature values were used to evaluate the XRD data of ChCl with a crystalline structure (Petrouleas, Lemmon, & Christensen, 1978). The fact that the free PLGA NPs showed no sharp peaks supported its amorphous nature (Khanal et al., 2016; Seju, Kumar, & Sawant, 2011). In the case of ChCl loaded NPs, the main peaks of choline chloride were absent and the ChCl loaded NPs exhibited the same characteristics as the free NPs, indicating that the ChCl loaded NPs were in a highly amorphous state and successfully encapsulated to NPs. There were no new sharp and broad peaks observed or no significant shift in the peaks and also the absence of a transition from amorphous to a crystalline character indicated that there was no ChCl on the surface after encapsulation (Yağci, Arvas, & Yazar, 2022).

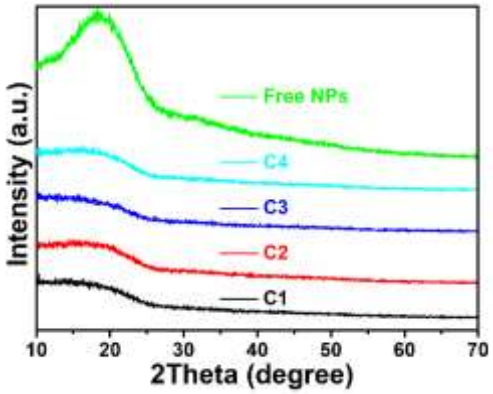

Figure 6. XRD spectra of the free and ChCl loaded (C1-C4) NPs

The in-vitro release profiles of the C1-C4 NPs were investigated to demonstrate ChCl's ability to reduce or increase drug release. As shown in Figure 7, initial burst release that was a well-known situation for PLGA NPs was detected in each formulation and 10-20% of the ChCl was released. It was thought that the highest release rate of the C4 formulation was due to the most negative zeta potential and thereby more interaction with the release buffer solution.

The general morphological features of the nanoparticles were evaluated with SEM imaging using only free nanoparticles. The SEM image of them was demonstrated in Figure 8. Although PLGA nanoparticles were damaged/melted because of exposure to the electron beam, especially in higher magnification, the particles were homogeneous and spherical and in the size range of 160 and 270 nm (Brauner et al., 2020). This supported the average size distribution of 261 nm obtained by the Zetasizer measurement.

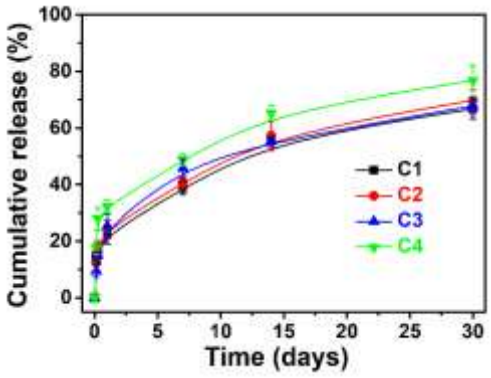

Figure 7. The in-vitro ChCl release profile of C1-C4 NPs

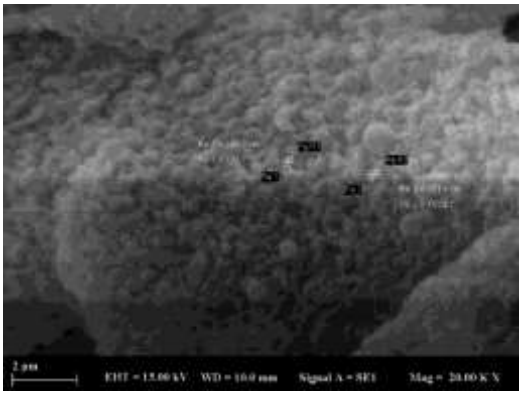

Figure 8. The SEM image of the free NPs at 20000x magnitude (scale bar: 2 µm)

3.2. Metal Labeling of the Nanoparticles

The obtained ChCl loaded NPs were labeled with Lu, Eu, and Gd metals. SEM-EDX analysis was performed on C1-C4 samples both to obtain information about the morphology of nanoparticles and to determine the metal content (Scimeca, Bischetti, Lamsira, Bonfiglio, & Bonanno, 2018; B. Ucar & Acar, 2021).

SEM imaging of each metal-labeled nanoparticle formulation was performed to examine whether the morphological properties of PLGA nanoparticles, as well as their distinctive spherical form and homogeneous distribution, changed after they were labeled with different metals.

In all metal labelings, according to semi-quantitative elemental analysis, the presence of metal in all nanoparticle formulations varying between 1% and 6% was detected (Figure 9-12).

The best labeling rate for Lu and Eu (6% and 3%, respectively) occurred in C4 nanoparticles, while C1 nanoparticles exhibited the highest labeling rate of Gd with 6%. The fact that the zeta potential in the C4 formulation was the most negative compared to the other formulations (C1-C3) may have resulted in more metal interaction. This may have provide the best labeling efficiency for Lu and Eu.

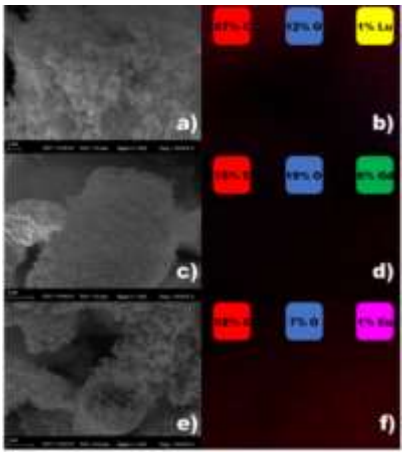

Figure 9. a, c, e) SEM images of C1 NPs labeled with Lu, Gd, and Eu, respectively at 20000x magnitude (scale bar: 1 µm for a, and 2 µm for c, and e). b, d, f) Elemental mapping of C1 NPs labeled with Lu, Gd, and Eu, respectively

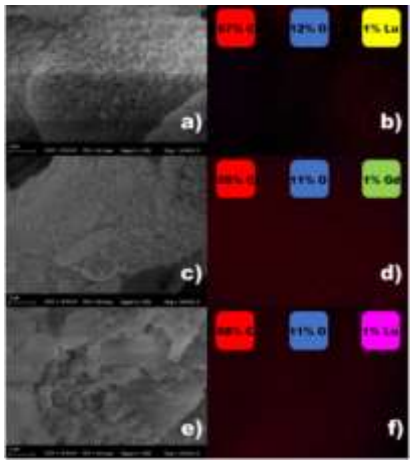

Figure 10. a, c, e) SEM images of C2 NPs labeled with Lu, Gd, and Eu, respectively at 20000x magnitude (scale bar: 2 µm). b, d, f) Elemental mapping of C2 NPs labeled with Lu, Gd, and Eu, respectively

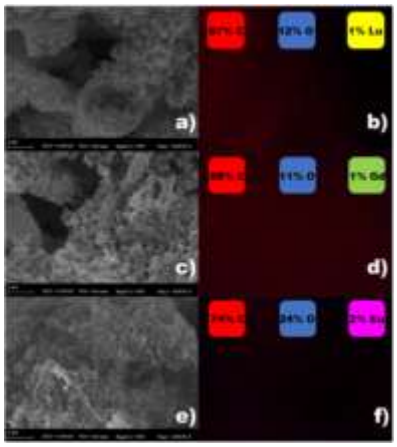

Figure 11. a, c, e) SEM images of C3 NPs labeled with Lu, Gd, and Eu, respectively at 20000x magnitude (scale bar: 2 µm). b, d, f) Elemental mapping of C3 NPs labeled with Lu, Gd, and Eu, respectively

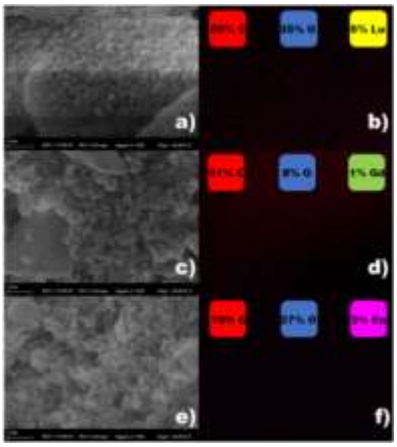

Figure 12. a, c, e) SEM images of C4 NPs labeled with Lu, Gd, and Eu, respectively at 20000x magnitude (scale bar: 2 µm). b, d, f) Elemental mapping of C4 NPs labeled with Lu, Gd, and Eu, respectively

4. Conclusions and Recommendations

In this work, ChCl was encapsulated into PLGA nanoparticles utilizing four different initial ChCl concentrations. Success of the nanoparticles formation and encapsulation process were proved by Zetasizer, LC-ESI-MS, FT-IR, SEM, and XRD analyses. The ChCl encapsulated nanoparticles were labeled with three natural lanthanide metals to simulate radiolabelling. Metal labeled nanoparticles were investigated morphologically with SEM and quantitatively with elemental mapping.

The results suggested that ChCl loaded PLGA nanoparticles can be easily labeled with different lanthanide group metals such as Lu, Eu, and Gd, and these developed procedures can also be easily applied with radioactive metals. Gadolinium, Lutetium and Europium labeled PLGA nanoparticles as choline carrier can be used both therapeutically and protectively against hepatic reticuloendothelial function injuries such as HCC, liver leak and cirrhosis. Different detection possibilities of these metals provides the opportunity to evaluate through different imaging modalities such as MRI, SPECT and fluorescent imaging. Thus, the targeted biological distribution and pharmacokinetic of the active substance can be followed more precisely and with higher accuracy.

5. Acknowledge

The author has declared no conflicts of interest.

References

Abamor, E. S., Allahverdiyev, A., Tosyali, O. A., Bagirova, M., Acar, T., Mustafaeva, Z., & Derman, S. (2019). Evaluation of in vitro and in vivo immunostimulatory activities of poly (lactic-co-glycolic acid) nanoparticles loaded with soluble and autoclaved Leishmania infantum antigens: A novel vaccine candidate against visceral leishmaniasis. *Asian Pacific Journal of Tropical Medicine*, *12*(8), 353-364.

Acar, T., & Ucar, B. (2022). Angiotensin (1-7)-Stearic Acid Conjugate: Synthesis and Characterization. *Journal of the Turkish Chemical Society Section A: Chemistry*, *9*(2), 331-338.

Al-Saeedi, F. J., & Cheng, B. (2013). Choline treatment affects the liver reticuloendothelial system and plasma fatty acid composition in diabetic rats. *Clinical Physiology and Functional Imaging*, *33*(4), 293-301.

Arias, N., Arboleya, S., Allison, J., Kaliszewska, A., Higarza, S. G., Gueimonde, M., & Arias, J. L. (2020). The relationship between choline bioavailability from diet, intestinal microbiota composition, and its modulation of human diseases. *Nutrients*, *12*(8), 2340.

Brauner, B., Semmler, J., Rauch, D., Nokaj, M., Haiss, P., Schwarz, P., . . . Gabor, F. (2020). Trimethoprim-loaded PLGA nanoparticles grafted with WGA as potential intravesical therapy of urinary tract infections—Studies on adhesion to SV-HUCs under varying time, pH, and drug-loading conditions. *ACS omega*, *5*(28), 17377-17384.

Cebeci, C., Ucar, B., Acar, T., & Erden, I. (2021). Colorimetric detection of hydrogen peroxide with gadolinium complex of phenylboronic acid functionalized 4, 5-diazafluorene. *Inorganica chimica acta*, *522*, 120386.

Cicalese, L. (2022). Hepatocellular Carcinoma (HCC). Retrieved from https://emedicine.medscape.com/article/197319-overview

Dangi, R., & Shakya, S. (2013). Preparation, optimization and characterization of PLGA nanoparticle. *International Journal of Pharmacy & Life Sciences*, *4*(7).

Dasari, S., & Patra, A. K. (2015). Luminescent europium and terbium complexes of dipyridoquinoxaline and dipyridophenazine ligands as photosensitizing antennae: structures and biological perspectives. *Dalton Transactions*, *44*(46), 19844-19855.

Dash, A., Pillai, M. R. A., & Knapp, F. F. (2015). Production of 177Lu for targeted radionuclide therapy: available options. *Nuclear medicine and molecular imaging*, *49*(2), 85-107.

Demirkol, M. O., Kiremit, M. C., Acar, O., Falay, O., Ucar, B., & Esen, T. (2018). Local salvage treatment of post-brachytherapy recurrent prostate cancer via theranostic application of PSMA-labeled lutetium-177. *Clinical genitourinary cancer*, *16*(2), 99-102.

Demirkol, M. O., Özkan, A., Uçar, B., Wester, H.-J., & Ferhanoğlu, B. (2021). Extramedullary Relapsed Multiple Myeloma Treatment With 177Lu-Labeled CXCR4 Endoradiotherapy and Dosimetric Results. *Clinical nuclear medicine*.

Gibellini, F., & Smith, T. K. (2010). The Kennedy pathway—de novo synthesis of phosphatidylethanolamine and phosphatidylcholine. *IUBMB life, 62*(6), 414-428.

Glunde, K., Bhujwalla, Z. M., & Ronen, S. M. (2011). Choline metabolism in malignant transformation. *Nature Reviews Cancer, 11*(12), 835-848.

Greiser, J., Weigand, W., & Freesmeyer, M. (2019). Metal-based complexes as Pharmaceuticals for Molecular Imaging of the liver. *Pharmaceuticals, 12*(3), 137.

Han, G., Deng, Y., Sun, J., Ling, J., & Shen, Z. (2015). Research into europium complexes as magnetic resonance imaging contrast agents. *Experimental and Therapeutic Medicine, 9*(5), 1561-1566.

Higdon, J., Drake, V., Delage, B., & Stocker, R. (2000). Linus Pauling Institute Micronutrient Information Center. *Oregon State University (2003–2018)*.

Khanal, S., Adhikari, U., Rijal, N. P., Bhattarai, S. R., Sankar, J., & Bhattarai, N. (2016). pH-responsive PLGA nanoparticle for controlled payload delivery of diclofenac sodium. *Journal of functional biomaterials, 7*(3), 21.

Kierkowicz, M., González-Domínguez, J. M., Pach, E., Sandoval, S., Ballesteros, B., Da Ros, T., & Tobias, G. (2017). Filling single-walled carbon nanotubes with lutetium chloride: A sustainable production of nanocapsules free of nonencapsulated material. *ACS Sustainable Chemistry & Engineering, 5*(3), 2501-2508.

Kuang, Y., Salem, N., Corn, D. J., Erokwu, B., Tian, H., Wang, F., & Lee, Z. (2010). Transport and metabolism of radiolabeled choline in hepatocellular carcinoma. *Molecular pharmaceutics, 7*(6), 2077-2092.

Lau, J. K. C., Zhang, X., & Yu, J. (2017). Animal models of non-alcoholic fatty liver disease: current perspectives and recent advances. *The Journal of pathology, 241*(1), 36-44.

Liu, Z.-Y., Yishake, D., Fang, A.-P., Zhang, D.-M., Liao, G.-C., Tan, X.-Y., . . . Zhu, H.-L. (2020). Serum choline is associated with hepatocellular carcinoma survival: a prospective cohort study. *Nutrition & metabolism, 17*(1), 1-9.

Llovet, J. M., Castet, F., Heikenwalder, M., Maini, M. K., Mazzaferro, V., Pinato, D. J., . . . Finn, R. S. (2022). Immunotherapies for hepatocellular carcinoma. *Nature Reviews Clinical Oncology, 19*(3), 151-172.

Makadia, H. K., & Siegel, S. J. (2011). Poly lactic-co-glycolic acid (PLGA) as biodegradable controlled drug delivery carrier. *Polymers, 3*(3), 1377-1397.

Marcolin, É., Forgiarini, L. F., Tieppo, J., Dias, A. S., Freitas, L. A. R. d., & Marroni, N. P. (2011). Methionine-and choline-deficient diet induces hepatic changes characteristic of non-alcoholic steatohepatitis. *Arquivos de gastroenterologia, 48*, 72-79.

Mehedint, M. G., & Zeisel, S. H. (2013). Choline's role in maintaining liver function: new evidence for epigenetic mechanisms. *Current opinion in clinical nutrition and metabolic care, 16*(3), 339.

NORD. (2017). Rare Disease Information / Hepatocellular Carcinoma. Retrieved from https://rarediseases.org/rare-diseases/hepatocellular-carcinoma/

O'Dwyer, C., Yaworski, R., Katsumura, S., Ghorbani, P., Gobeil Odai, K., Nunes, J. R., . . . Han, S. (2020). Hepatic Choline Transport Is Inhibited During Fatty Acid–Induced Lipotoxicity and Obesity. *Hepatology communications, 4*(6), 876-889.

Özkan, A., Uçar, B., Seymen, H., Yarar, Y. Y., Falay, F. O., & Demirkol, M. O. (2020). Posttherapeutic critical organ dosimetry of extensive 177Lu-PSMA inhibitor therapy with metastatic castration-resistant prostate cancer: one center results. *Clinical nuclear medicine, 45*(4), 288-291.

Petrouleas, V., Lemmon, R., & Christensen, A. (1978). X-ray diffraction study of choline chloride's β form. *The Journal of Chemical Physics, 68*(5), 2243-2246.

Philips, C. A., Rajesh, S., Nair, D. C., Ahamed, R., Abduljaleel, J. K., & Augustine, P. (2021). Hepatocellular carcinoma in 2021: an exhaustive update. *Cureus, 13*(11).

Scimeca, M., Bischetti, S., Lamsira, H. K., Bonfiglio, R., & Bonanno, E. (2018). Energy Dispersive X-ray (EDX) microanalysis: A powerful tool in biomedical research and diagnosis. *European journal of histochemistry: EJH, 62*(1).

Seju, U., Kumar, A., & Sawant, K. (2011). Development and evaluation of olanzapine-loaded PLGA nanoparticles for nose-to-brain delivery: in vitro and in vivo studies. *Acta biomaterialia, 7*(12), 4169-4176.

Sivrikaya, S. (2019). A novel vortex-assisted liquid phase microextraction method for parabens in cosmetic oil products using deep eutectic solvent. *International Journal of Environmental Analytical Chemistry, 99*(15), 1575-1585.

Snehalatha, M., Venugopal, K., Saha, R. N., Babbar, A. K., & Sharma, R. K. (2008). Etoposide loaded PLGA and PCL nanoparticles II: biodistribution and pharmacokinetics after radiolabeling with Tc-99m. *Drug delivery, 15*(5), 277-287.

Tikhonova, T. N., Shirshin, E. A., Budylin, G. S., Fadeev, V. V., & Petrova, G. P. (2014). Assessment of the europium (III) binding sites on albumin using fluorescence spectroscopy. *The Journal of Physical Chemistry B, 118*(24), 6626-6633.

Tosyali, O. A., Allahverdiyev, A., Bagirova, M., Abamor, E. S., Aydogdu, M., Dinparvar, S., . . . Derman, S. (2021). Nano-co-delivery of lipophosphoglycan with soluble and autoclaved leishmania antigens into PLGA nanoparticles: Evaluation of in vitro and in vivo immunostimulatory effects against visceral leishmaniasis. *Materials Science and Engineering: C, 120*, 111684.

Ucar, B. (2019). Synthesis and characterization of natural lanthanum labelled DOTA-Peptides for simulating radioactive Ac-225 labeling. *Applied Radiation and Isotopes, 153*, 108816.

Ucar, B., & Acar, T. (2021). Macroaggregated Albumin (MAA): Production, Size Optimization, Eu (III) and Tb (III) Complexes. *Journal of the Turkish Chemical Society Section A: Chemistry, 8*(1), 209-216.

Ullah, R., Atilhan, M., Anaya, B., Khraisheh, M., García, G., ElKhattat, A., . . . Aparicio, S. (2015). A detailed study of cholinium chloride and levulinic acid deep eutectic solvent system for CO 2 capture via experimental and molecular simulation approaches. *Physical Chemistry Chemical Physics, 17*(32), 20941-20960.

WHO. (2020). International Agency for Research on Cancer, Estimated number of new cases in 2020, all cancers, both sexes, all ages.

Willyard, C. E., & Kalathil, S. C. (2020). Nuclear Medicine Liver/Spleen Test.

Yağci, Ö., Arvas, M. B., & Yazar, S. (2022). Facile and single step produced Ba: Sn-codoped PEDOT: PSS thin film electrode with improved optics and electrochemical properties for transparent and flexible supercapacitor applications. *New Journal of Chemistry, 46*(46), 22130-22142.

Yazar, S., Arvas, M. B., & Sahin, Y. (2022). Hydrothermal Synthesis of Flexible Fe-Doped Polyaniline/Dye-Functionalized Carbon Felt Electrode for Supercapacitor Applications. *ChemistrySelect, 7*(21), e202200016.